Available online at www.sciencedirect.com
ScienceDirect
Journal of the European Ceramic Society 28 (2008) 393–400
www.elsevier.com/locate/jeurceramsoc

Hydrogen bonding and diffusion in mullite

Claus H. Rüscher [a,*], Nadine Eils [a,b], Lars Robben [a], Hartmut Schneider [b]

[a] *Institute for Mineralogy and ZFM, Leibniz University Hannover, Welfengarten 1, 30167 Hannover, Germany*
[b] *German Aerospace Center, Institute of Materials Research, 51147 Köln, Germany*

Available online 25 April 2007

Abstract

Traces of OH groups have been identified in the infrared absorption spectra of a nominally anhydrous synthetic mullite single crystal. The OH absorption profiles were resolved with four peaks for polarizations *E*//*a*, *E*//*b* and *E*//*c*, respectively. The integrated absorption intensities correspond to an H_2O content of about 10 ppm (wt) using an average extinction coefficient according to the mean wavenumber relation. The length of O_1–H···O_2 bonds (O_1–H hydroxyl groups with hydrogen bridging towards a neighboring oxygen, O_2) range between 276 and 314 pm following empirical relations for hydrogen bonding in aluminosilicates. According to lattice energy calculations the infrared peak positions can be associated with two different classes of hydrogen positions assuming a substitution $Si^{4+} \Leftrightarrow 4H^+$: one type of H atoms is bound on tetrahedral faces of substituted Si-sites involving intense O_1–H···O_2 hydrogen bridging. A second type of H atoms form more isolated O–H groups directed into the structural channels of mullite running along the crystallographic *c* axis. These OH dipoles show polarizations perpendicular to the *c* axis. A third type of OH dipole is oriented parallel to the *c* axis and could be assigned to appropriate pairs of oxygen in two neighboring unit cells, e.g. O_{c1}–H···O_{c2}.

Heating experiments for 12 h at 1200 °C, 6 h at 1300 °C and 4 h at 1400 °C reveal a significant decrease of OH concentration on ppm level. OH absorption profiles measured on cross-sections by infrared microscope technique yielded for example at 1300 °C diffusion coefficients of $D_a \approx D_b \approx 8 \times 10^{-9}$ (parallel to the *a* and *b* axis) and $D_c \approx 1.5 \times 10^{-8}$ cm^2/s (parallel to the *c* axis). The observation $D_c > D_a \approx D_b$ corresponds to a preferred diffusion parallel to the structural channels in *c* direction. The temperature dependence of the diffusion coefficient D_c of hydrogen outward diffusion is described with an Arrhenius activated behavior (190 kJ/mol). It includes the diffusion coefficient of hydrogen inward diffusion, which was obtained by submitting originally H-free mullite at 1670 °C to a water-rich atmosphere.

Keywords: Drying; Impurities; Diffusion; Mullite; Functional Applications

1. Introduction

During the past decades numerous studies have demonstrated that natural and synthetic nominally anhydrous samples can incorporate significant traces of OH species.[1–5] Hydrous components in rock-forming nominally anhydrous minerals of the earth mantle are very important for the understanding of many geological processes concerning melt viscosity, crystallization processes and the global cycle of hydrogen.[6–8] A comprehensive overview of properties of water in nominally anhydrous minerals has been published recently.[9] Investigations of the OH incorporation and OH content in the technical important materials like quartz, α-alumina and α-alumina ceramics show that there exists a strong correlation between OH incorporation and the mechanical properties.[10–12]

Mullite is an important phase in ceramics used for high temperature applications.[13,14] Traces of OH formation were observed in initially OH-free crystals after treatment in water vapor-rich high temperature (1600 °C) environments.[15] Eils et al.[16] related the formation of OH to bond breaking effects of Si–O–Al by H_2O involving diffusion of H and/or OH species, and to a counter diffusion of positively charged impurities (Li, Na). According to recent results with the micro-spot LA-ICP-MS technique (laser ablation inductive coupled mass spectrometry) an impurity counter diffusion mechanism can be ruled out.[17] These studies provided evidence for an inward but no outward diffusion of Na and also of Mg. The foreign cations are enriched in melt bottles at the surface of mullite indicating a significant contamination coming from the furnace atmosphere in these types of experiments. Charge compensation of inward migrated H, Na, and Mg atoms can be achieved via the addition of O^{2-} anions through anion defects. Another even more likely compensation mechanism suggests an equivalent defect formation on cation sites of the form $Si^{4+} \Leftrightarrow 4H^+$, $Si^{4+} \Leftrightarrow Na^+ + 3H^+$, $Al^{3+} \Leftrightarrow 3H^+$, etc.[18]

For a better understanding of these complex processes, it is necessary to investigate the H bonding (OH formation) in mul-

* Corresponding author.
E-mail address: c.ruescher@mineralogie.uni-hannover.de (C.H. Rüscher).

0955-2219/$ – see front matter © 2007 Elsevier Ltd. All rights reserved.
doi:10.1016/j.jeurceramsoc.2007.03.018

lite in more detail. A standard method to analyze OH species, i.e. their quantification and structural bonding, is infrared absorption spectroscopy, using empirical relations in both cases[19–22] which is applied here. This investigation is focussed on mullite single crystal plates prepared from a suitable as grown single crystal which contains already suitable OH concentration homogeneously distributed in the as received state. Specimens were specially designed in order to enable cross-section measurements in two independent directions of outward diffusion profiles by microscope technique. Thereby an accurate determination of the anisotropic diffusion coefficients is possible. Due to the close structural similarities of mullite and sillimanite, the latter has been included in the discussion.

2. Experimental details

For the experiments a single crystal containing OH in the as received state grown by the group of S. Uecker (Institute for Crystal Growth, Berlin-Adlershof, Germany) using the Czochralski technique. Crystal plates cut from this material was also used in previous studies[16] together with a mullite single crystal which does not show OH in equivalent thick plates in the as received state. It was analyzed that the chemical composition of the mullite single crystals corresponds closely to 2/1-mullite ($2Al_2O_3{\cdot}1SiO_2$; *Pbam*; $a = 758$ pm, $b = 768$ pm, $c = 289$ pm).

For the heating experiments plane parallel crystal plates of size 5 mm × 5 mm × 1.7 mm were used. For the determination of the anisotropic diffusion coefficients single crystals plates were cut into cuboids with edge length of about 1.7 mm × 1.7 mm × 5 mm. The surfaces were polished to high optical quality as described earlier.[16] The cuboid samples were placed into a platinum crucible which has the form of a one side open cylinder of 5 mm diameter and 8 mm height. The plate samples were placed as a hut on top of the crucible. Heating times were 4, 6 and 12 h at $T_k = 1400$, 1300 and 1200 °C, respectively, using different atmospheric conditions. For the experiment at 1200 °C a standard furnace (Nabertherm L08/14 equipped with a C 19 program controller) was used and the sample was heated in usual air conditions of the oven. The other experiments were carried out under well-defined conditions using a TG/DTA (thermo gravimetrical/differential thermal analyzer) controlled device (Setaram setsys evolution 1650). Before starting an experiment the sample chamber was evacuated and then filled with He. During the experiments a constant He flow rate of 50 ml/min was conducted. A heating/cooling rate of 15 °C/min was used in the range between 20 and 1000 °C and of 20 °C/min between 1000 °C and T_k.

All specimens were investigated by optical microscopy and polarized infrared spectroscopy (IR) in the range between 400 and 7000 cm^{-1}. Orientations were determined by infrared spectra in reflection mode according to the known components.[23–25] For standard measurements crystal plates of suitable size were measured under evacuated conditions (Bruker IFS 66v, MCT detector and DTGS detector) using mm sized well defined apertures. Smaller sized specimen and profile measurements were investigated by microscope technique (Bruker IFS 88 with attached microscope IR scope II and equipped with an MCT/InSb sandwich detector cooled by liquid nitrogen) before and after the heat treatment. For the determination of diffusion profiles cross-sections of suitable thicknesses (see below) were cut perpendicular to the plate surface and for the cuboids perpendicular to the long extension of the specimen axis with defined main orientation. Surfaces were also polished to high optical quality. Spectra were taken with rectangular apertures of 0.1 mm × 0.01 mm using polarized light (KRS 5) in an analogous way as described in the earlier diffusion profile measurements.[16] Further information of polarization dependences are given in the text below.

Sillimanite specimen were cut from gem grade optically clear sillimanite single crystals of locality Sri Lanka and are of the same origin as used in previous study[24] which were characterized by IR reflection spectra and XRD data ($a = 748.8$ pm, $b = 768.1$ pm, $c = 577.7$ pm in *Pbnm* equivalently oriented to mullite).

3. Results and discussion

3.1. Hydrogen bonding in mullite

The infrared absorption (IR) spectra of 2/1-mullite single crystals in the as received state display a significant OH content. The OH groups are homogeneously distributed through the crystal plates. The IR spectra measured for polarizations *E*//*a* and *E*//*b* are in good agreement with the results obtained from all measurements of water vapor (at 1670 °C) treated samples being free of OH in the as received state.[16] This implies that hydrogen bonding is essentially of the same type in all mullite samples investigated so far. Also the new measurements of the *E*//*c* component agree with spectra from mullite treated at high temperature in water-rich atmosphere.[15] An overview of all OH absorption characteristics is shown in Fig. 1 with the Lorentzian profile analyses. As can be seen a very good agreement between measured and least square fitted Lorentzian is obtained using a minimum of four peaks for each component. The values of the fit are given in Table 1. As shown by Eils et al.[16] for the *E*//*a* and *E*//*b* spectra, an additional peak for the *E*//*c* component compared to the earlier result by Rüscher et al.[15] has to be taken into account, too.

Knowing the total intensity of the OH absorption the total OH content was estimated using the Lambert–Beer law:

$$c(H_2O, \text{wt\%}) = \frac{1.802 A_i}{d \varepsilon_i \rho_M} \quad (1)$$

where A_i is the integral absorption, d the sample thickness (cm), ρ_M the density of mullite: 3.166 g/cm^3 and ε_i is the integral molar absorption coefficient in (l mol^{-1} cm^{-2}).

Since the specific single peak absorption coefficients are unknown for mullite a "mean wavenumber relation" has been used for the integral molar absorption coefficient following Libowitzky and Rossman[26] as

$$\varepsilon_i = 246.6(3753 - \nu), \quad \nu = \frac{\sum \nu_j A_{ij}}{\sum A_{ij}} \quad (2)$$

Table 1
Results of Lorentzian peak fitting of OH profiles of polarizations *E//a*, *E//b*, and *E//c*

Peak	Peak position (cm^{-1})	Peak height (cm^{-1})	Damping (cm^{-1})	Integral intensity (cm^{-2})	O_1–H···O_2 (pm)	H···O_2 (pm)
E//a						
1	3346	0.02	119	4	277	188
2	3448	0.11	100	18	284	197
3	3550	0.07	66	8	300	214
4	3600	0.09	58	8	∞	235
E//b						
1	3370	0.02	132	4	278	190
2	3460	0.16	107	27	285	199
3	3537	0.17	73	20	296	211
4	3592	0.07	40	4	∞	230
E//c						
1	3367	0.02	180	6	278	189
2	3457	0.07	100	10	285	198
3	3510	0.09	76	10	291	206
4	3577	0.02	45	2	314	223

O_1–H···O_2 and H···O_2 distances are calculated using peak positions and Eqs. (4) and (5), given further in the text below.

where ν is the mean wavenumber of the OH stretching bands, ν_j the wavenumber for peak j and A_{ij} is the peak area for peak $i = 1, 2, 3$; $j = 1, 2, 3, 4$.

The calculation reveals an absolute H_2O content of about 10 ppm for the mullite single crystals containing OH in the as received state. The components for *E//a*, *E//b* and *E//c* contribute to about 32, 55 and 23%, respectively, to the total OH content of the mullite. Each component of the OH spectra (Fig. 1) may enclose a significant distribution of OH dipoles according to the complex real structure of mullite.[13,14,28] The data in Table 1 collects the results using a minimum number of four peaks for each direction which provides a suitable approximation of the spectra. The question is if each of the four peaks belongs to a component of the same OH dipole. In an orthorhombic crystal matrix containing an isolated OH dipole of fixed frequency and defined orientations to the crystallographic axis the relative intensity contribution for *E//a*, *E//b* and *E//c* can be used for the determination of their orientation according to[27]:

$$\frac{I_a}{I_{tot}} = \cos^2(\Theta_a), \qquad \frac{I_b}{I_{tot}} = \cos^2(\Theta_b), \qquad \frac{I_c}{I_{tot}} = \cos^2(\Theta_c),$$
$$\text{and} \quad I_{tot} = I_a + I_b + I_c \tag{3}$$

where $I_{a,b,c}$ are the absorption peak intensities of the OH dipole parallel to the a, b and c axis and $\Theta_{a,b,c}$ are the angles of the OH dipole axis relative to the a, b and c axis. Since the half width of the peaks becomes very large for peaks 1 and 2 their peak position seems to be most uncertain compared to those of peaks 3 and 4 in Table 1. It may be suggested that peak 1 coincides in peak position for *E//a*, *E//b* and *E//c*. The same could be true for peak 2. Therefore, the appropriate (average) orientations of OH dipole axes towards the crystallographic axis may be calculated using Eq. (3) for peak 1 ($\Theta_{a,b,c} = 57°, 59°, 48°$) and for peak 2 ($\Theta_{a,b,c} = 55°, 45°, 64°$). Similarly the peak 4 could be adjusted to the same maximum position implying major components in *E//a* and *E//b* and a smaller one in *E//c*, revealing $\Theta_{a,b,c} = 40°$, 57°, 71°. Assuming that peak 3 of *E//a* and *E//c* coincides which suggests an orientation of about 45° with respect to the a and b directions with a negligible component parallel c. On the other hand peak 3 of *E//c* does not show any counterpart in *E//a* and *E//b* which implies an orientation parallel to c. According to this there are "only" five different OH dipoles of distinct main orientations in mullite. However we may also note, that the qual-

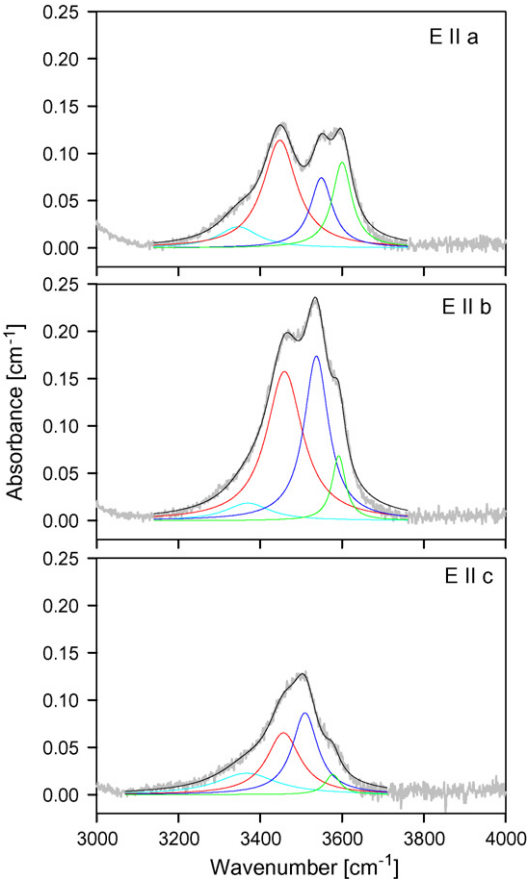

Fig. 1. Infrared absorption spectra in the range of OH stretching excitation of mullite for polarizations *E//a*, *E//b*, and *E//c* (scattered line) and results of Lorentzian curve fitting with four peaks and their sum spectra (solid lines) for each component.

ity of fit becomes less good using fixed average peak positions. Increasing the number of peaks was also unsuccessful.

Using further on as one parameter the empirical relations for the effective hydrogen bonding O_1–H···O_2 (O_1–H and H···O_2 denote the shorter and longer length in a hydrogen bond) and the long H···O2 distances (both in pm) as given by Libowitzky[22]:

$$w_{OO}\,(\mathrm{cm}^{-1}) = 3592 - 304 \times 10^9 \exp\left(\frac{-\langle \mathrm{O1{-}O2}\rangle}{13.21}\right) \quad (4)$$

$$w_{HO}\,(\mathrm{cm}^{-1}) = 3632 - 1.79 \times 10^6 \exp\left(\frac{-\langle \mathrm{H\cdots O_2}\rangle}{21.46}\right) \quad (5)$$

the frequencies would correspond to values in the range between 276 and 314 pm and between 188 and 235 for w_{OO} and w_{HO}, respectively (Table 1). A possible way of finding the proton sites is to compare all O–O distances of mullite and the suggested dipole orientations which may separate specific localization of protons in the structure. A similar strategy was followed by Stalder[29] for OH formation in enstatite. Following this for mullite the calculated O_1–O_2 (Table 1) are consistent with O–O distances on the faces of the tetrahedron (T) type polyedron (277–288 pm) and longer distances involving neighbouring oxygen through the channels (293–312 pm) (for structural details compare Angel and Prewitt[28]). According to Eq. (4) peak 3 in *E*//*c* corresponds to a linear O_1–H···O_2 distance of 291 pm, which is very close to the *c* lattice parameter of 2:1 mullite (289 pm). Therefore, this peak could be assigned to proton localizations between corresponding oxygen pairs of two neighboring unit cells along *c*, e.g. as O_{c1}–H···O_{c2} along the tetrahedral double chains (see below).

Sillimanite, $Al_4Si_2O_{10}$, is structurally and chemically closely related to mullite, $Al_{4+2x}Si_{2-2x}O_{10-x}$. Both minerals are characterized by chains of edge-connected [AlO_6] octahedral running parallel to the crystallographic *c* axis. The octahedral chains are linked by (Al,Si)O_4 tetrahedral double chains with ordered Al and Si in the case of sillimanite. For mullite the double chains are disturbed in a way that a number of Si is substituted by Al formally described by $2Si^{4+} + O^{2-} \Rightarrow 2Al^{3+} + V$ (V = oxygen vacancy). This means that for charge compensation a bridging oxygen of the tetrahedral double chains becomes removed (V) and related tetrahedral cations are moved to new T* sites. 2:1 mullite, $x = 0.25$, contains one oxygen vacancy per four unit cells. It is interesting to compare the sillimanite OH absorption spectra to those of mullite as shown in Fig. 2. The sillimanite spectra are in very good agreement with the results of earlier investigations,[30,31] both in peak positions and anisotropy and even tentatively in the order of magnitude of total absorption. From heating experiments Beran et al.[31] estimated a maximum amount of bound OH in sillimanite of about 200 ppm (wt, H_2O). Compared to sillimanite the total OH absorption intensity for the mullite is lower, corresponding to 100 ppm (wt, H_2O) for the here measured sillimanite. Beran et al.[30] assigned the *E*//*a* polarized peaks between 3200 and 3300 cm^{-1} to Al vacancies on tetrahedral sites (Al_2) and corresponding hydrogen bridging along the "Al_2"O_4-tetraeder edge (O_b–O_c) being about 289 pm in length. The peak at 3550 cm^{-1} has components in *E*//*a* and *E*//*b*. The corresponding OH dipole could be oriented from one O_b position near an empty tetrahedral site Al_2 to another O_b in a further distance away (*b*/2).[30] This implies that the bridging O_{1b}–H···O_{2b} is weaker (higher wavenumber peak) compared to the O_{1b}–H···O_c one (lower wavenumber peaks). Natural sillimanite contains significant amounts of impurities, e.g. Fe, Cr,[30] and the OH absorptions could be influenced by such substitutions[29] for the strong peaks between 3200 and 3300 cm^{-1} and at 3550 cm^{-1}. For mullite OH absorption occurs between 3350 and 3600 cm^{-1}. It could be associated to similar absorption peaks of sillimanite which underlie the strong peak at 3550 cm^{-1} but could not further be separated.

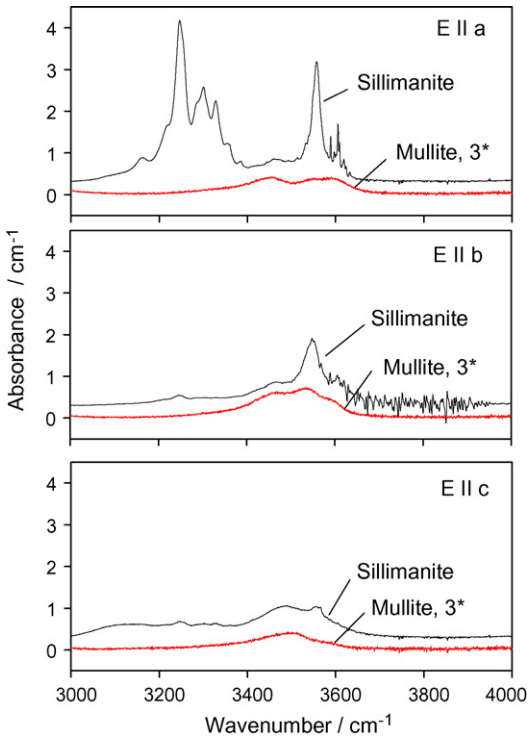

Fig. 2. Mullite spectra for *E*//*a*, *E*//*b*, and *E*//*c* from Fig. 1 compared to corresponding components of sillimanite single crystal plates (gem quality). Note that the mullite spectra were multiplied by a factor of 3 for better comparison.

Ab initio molecular orbital calculations on a variety of hypothetical aluminosilicate molecules by Kubicki et al.[21] reveal interesting correlations of OH frequencies and O_1–H···O_2 distances and angles which have to be taken into account for the use of empirically determined relations. The results may be summarized as follows:

i. The OH frequency decreases linearly between 2100 and 3800 cm^{-1} for a variation in O_1–H length between 104 and 92 pm.
ii. For H···O_2 distances larger than 200 pm the OH frequency dependence is cut off above about 3750 cm^{-1}.
iii. O_1–H···O_2 bonding angles larger than 100° produce a broader range of OH frequencies as compared to OH vibrations with smaller angles. Also, larger angles allow for stronger H bonding, which means that frequency shifts can be larger with increasing angles.

Table 2
O_1–H···O_2 distances and angles of energy minimized 2 × 2 × 2 sillimanite unit cell with an exchange of $1Si^{4+} \Leftrightarrow 4H^+$ using GULP

Hydrogen	Position	O_1–H (pm)	O_2–H (pm)	O1···O2 (pm)	Angle O_1–H–O_2 (°)	OH-dipole angle with respect to *a*/*b*/*c*
H1	T*	114.9	156.0	259.5	146	25.9/73.5/70.1
H2	T*	112.9	166.8	271.6	151	79.0/49.9/42.2
H3	Terminal	105.2	211.1	284.7	125	18.6/71.7/86.8
H4	Terminal	99.7	201.4	264.2	118	64.6/25.6/87.1

The absolute energy arrived at −1147.22 eV (unrelaxed lattice) compared to the fully optimized sillimanite structure of −1155.19 eV, which well agree to published data for sillimanite. T*: proton close to tetrahedral site where the Si^{4+} has been before.

iv. Correlations among H bond distances, O_1–H···O_2 angles and O_1–H bond lengths can obscure the effect of any one parameter calculation on vibrational frequencies.

From our observations of peak positions between 3600 and 3346 cm^{-1} and according to the relation in (i) imply O1–H bond length between 95 and 99 pm. For a further understanding of the hydrogen bonding in mullite some first steps of calculations were carried out using the computer program GULP.[32] The basic idea was to start from a 2 × 2 × 2 sillimanite lattice cell and to substitute one Si^{4+} by $4H^+$ with some arbitrary placements. The preliminary results show (Table 2) a very good energy minimum. The final result is shown in Fig. 3. Two protons (H1/H2) are localized within the vacancy—or to be more accurate, they occupy sites on the tetrahedron faces. Two further protons (H3/H4) are localized within the channels running parallel to the *c* axis of mullite (Fig. 3). Following these results peaks 1 and 2 (Table 1) can be assigned to stronger hydrogen bridges between oxygen on tetrahedral faces whereas peaks 3 and 4 are assigned to O–H dipoles directed into the channel. The calculations show optimised O_1–H lengths (Table 2) of 115/113 pm (H1/H2) and 105/100 pm (H3/H4) related to OH dipoles in tetrahedral sites and terminal directed OH, respectively. Conclusively H1/H2 and H3/H4 possess stronger and weaker hydrogen bonding, respectively. Additionally it comes out that the latter OH bonds are polarized with components parallel to the (0 0 1) planes whereas the former show angles between 30° and 80° with respect to the direction of the crystallographic axis. Similar observations were discussed above. The results of these calculation cannot explain a dipole orientation parallel to the crystallographic *c* axis implied by peak 3 for *E*//*c*, which becomes, however, not energetically favourable.

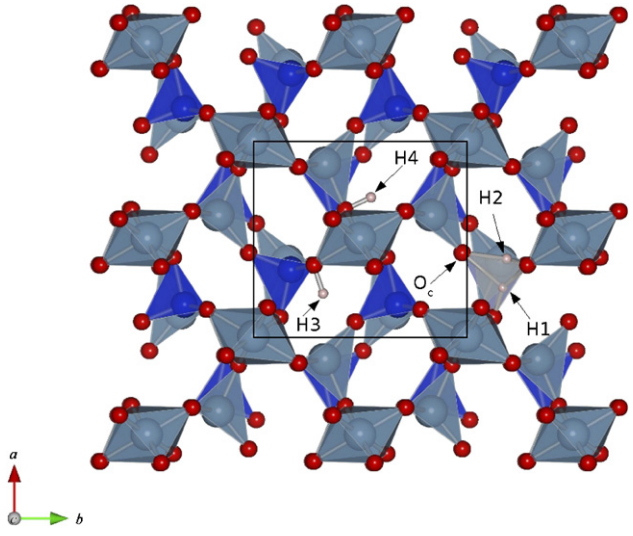

Fig. 3. Projection of an energy minimized 2 × 2 × 2 sillimanite structure along *c* including an exchange of $1Si^{4+} \Leftrightarrow 4H^+$ using GULP (compare Table 2 and text). Shown are the hydrogen localizations H1–H4 and the sillimanite tetrahedra and octahedra units.

3.2. Hydrogen diffusion in mullite

Investigations on the hydroxylation of mullite single crystal (0 0 1) plates have shown a significant inward diffusion of species within short periods of times (<12 h) at high temperature in a water-rich slowly flowing reaction atmosphere.[15,16] Dry conditions at the end of the experiment indicated strong outward diffusion profiles. This implies immediately that a mullite sample containing homogeneously distributed OH groups as characterized above can be used for quantifications of outward diffusion profiles arrived in systematic investigation under dry conditions. Results of such investigations are collected in Figs. 4–7. Diffusion data were calculated according to the solution of Fick's second law for a constant surface concentration[33] at different temperatures:

$$n(x) = (n_0 - n_s)\,\mathrm{erf}\left(\frac{x}{2\sqrt{Dt}}\right) + n_s \quad (6)$$

where *n* is the concentration, n_0 the concentration in the bulk, n_s the concentration at the surface, *x* the distance, *D* the diffusion coefficient and *t* is the time.

Calculated diffusion curves are shown for one half of the specimen (Figs. 4, 5 and 7). In a first step relatively large (0 0 1) crystal plates (5 mm × 5 mm × 1.7 mm) were used for diffusion experiments parallel to the *c* axis (D_c). Diffusion profiles were measured in cross-sections of the crystal cut parallel to the *b* axis being heated at 1200 °C (12 h) and 1300 °C (6 h), which are given in Fig. 4 (top and bottom), respectively. The profiles were measured for the absorption components with the electrical field polarized parallel to the *b* axis. The level of sensitivity was sufficiently increased by measuring the change in spectra relative to the midpoint of the profile section and calibrating the absolute value to the spectra of the untreated mullite given in Fig. 1. The intensities given in Figs. 4–7 are taken at a fixed frequency, which is useful since the shape of the absorption characteristics remains essentially the same over the crystal. There is a clear plateau of the intensity in the middle of the crystal (Fig. 4). As verified

by the calculation using Eq. (3) the plateau indicates no loss of OH concentration in this part of the crystal. The calculated absolute value of the diffusion coefficient depends sensitively on the concentration variation close to the surface in the range 0.1–0.2 mm which is difficult to obtain with higher accuracy than ±50% of the absolute value. Another reason for surface alteration of the mullite plates during the heating experiments certainly is contamination from the furnace atmosphere. If, for example mullite is annealed in air furnaces in alumina tubes and alumina crucibles often local surface melting and recrystallization of α-alumina within such melt bottles is observed.[16,17] This effect is not restricted to water-rich slowly flowing atmosphere but can also be seen in dry air conditions as well (photograph inside Fig. 4, top). On the other hand, in high temperature inert gas experiments (e.g. He atmosphere), the surface alteration is reduced the cleaner the total environment is. The very weak surface alteration observed typically in such type of experiments is shown in the photograph inside Fig. 4 (bottom).

Further diffusion experiments were carried out using samples cut into cuboids of 1.7 mm × 1.7 mm × 5 mm in size. This technique enables diffusion profile evaluation for the determination of diffusion components of sufficient high precession in two directions perpendicular to the long extension of the specimens (Figs. 5–7). Strong anisotropic diffusion is obtained at 1300 °C with $D_c = 1.5 \times 10^{-8}$ cm²/s being much larger compared to $D_a = 8 \times 10^{-10}$ cm²/s (Fig. 5). Presently we cannot explain the difference of the outward diffusion curves parallel to *c* near the surface under the same conditions (6 h, 1300 °C) for the cuboid and platy sample (Figs. 5 and 4, bottom). The different curves could be related to different surface related effects but also to changes in the diffusion mechanism during the experiment. However, both profile forms can be described with the same diffusion coefficient. A strong anisotropy with $D_a < D_c$ is observed in the 1400 °C samples, too (Fig. 6, compare profiles for diffusion //*a* and //*c* at 4 and 5 h, respectively). Additionally the results obtained from the 3 and 4 h experiments show the time dependent progress of diffusion. In diffusion experiments parallel *c* (*D*//*c*) there is evidence that the diffusion slows down with time. Tentative calculations using Eq. (6) yield a diffusion coefficient $D_c \approx 3 \times 10^{-8}$ cm²/s ignoring the flattening effect towards the surface. For diffusion parallel to the *a* axis a value of $D_a \approx 8 \times 10^{-9}$ cm²/s is estimated. It is interesting to see that for the diffusion parallel to *a* and *b* any anisotropy is within the experimental error with a calculated diffusion coefficient of $D_{a,b} \approx 9 \times 10^{-9}$ cm²/s (Fig. 7).

The obtained diffusion coefficients from outward diffusion experiments (depletion of OH) are collected in Fig. 8 together with earlier results obtained at higher temperature for inward

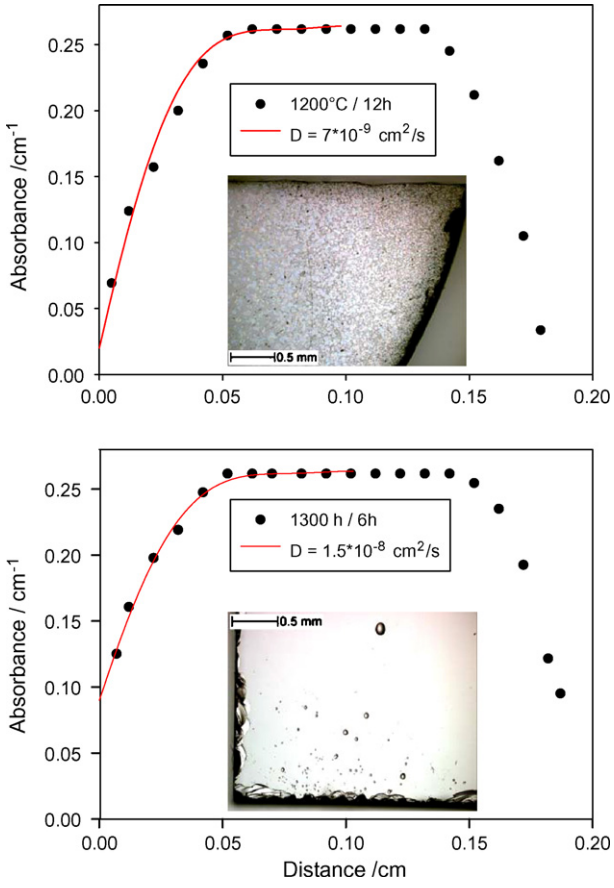

Fig. 4. Absorption profiles for diffusion component D_c as measured for polarization *E*//*b* of cross-section cut from mullite (0 0 1) plates heat treated at 1200 °C/12 h (top) and 1300 °C/6 h (bottom) as denoted. Solid lines show profile calculation using Eq. (6) and diffusion coefficient as given. Optical micrographs inside show the plates after the heating experiment in air furnace atmosphere (1200 °C) and under flowing He (1300 °C), respectively.

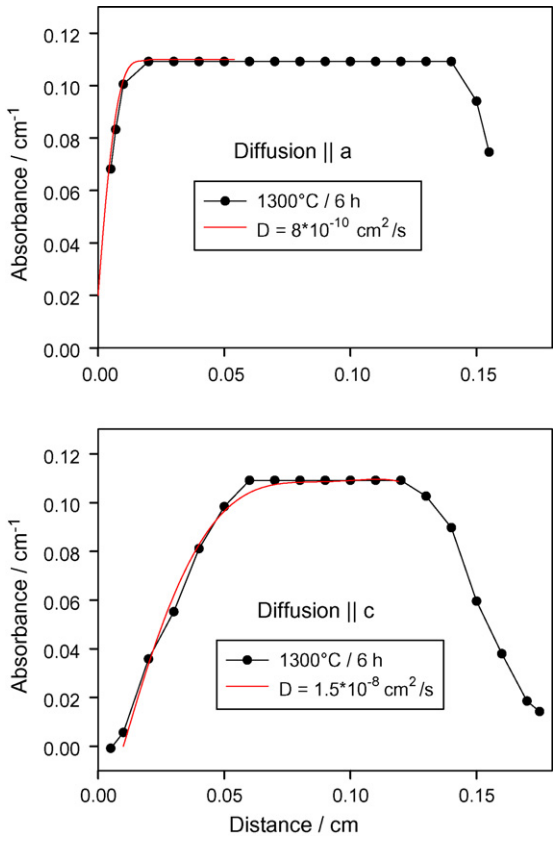

Fig. 5. Absorption profiles for diffusion components D_a (top) and D_c (bottom) as measured for polarization *E*//*a* of cross-section cut from mullite [0 1 0] cuboids heat treated at 1300 °C/6 h, in flowing He. Solid lines shows profile calculation using Eq. (6) and diffusion coefficient as given (note different thicknesses of cross-section for D_a and D_c).

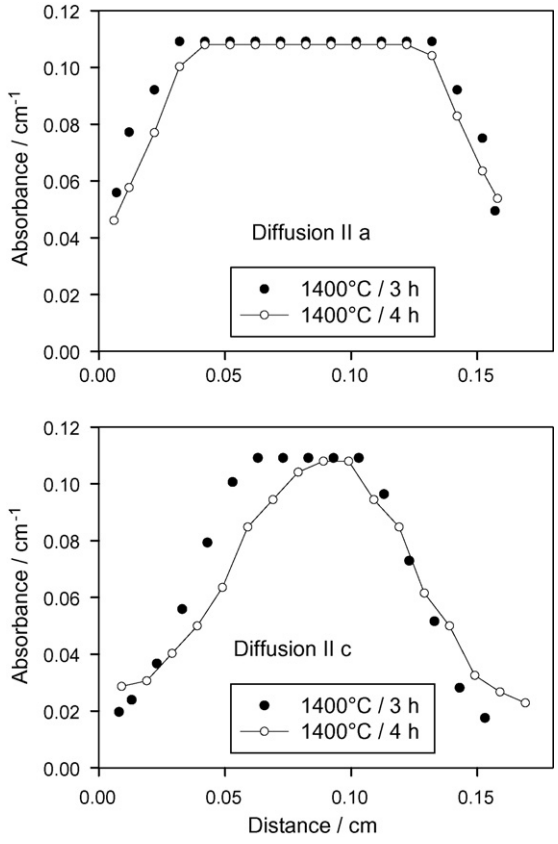

Fig. 6. Absorption profiles for diffusion components D_a (top) and D_c (bottom) as measured for polarization $E//a$ of cross-section cut from mullite [0 1 0] cuboids heat treated at 1400 °C/3 h (closed symbols) and 1400 °C/4 h (open circles, connected by solid line). Note individual length in each case, the systematically advanced diffusion for the 4 h with respect to the 3 h treatment and for diffusion parallel to c, compared to diffusion parallel to a.

diffusion[16] and for ^{18}O, ^{26}Al, and ^{30}Si tracer diffusion experiments by Fielitz et al.[34] It can be seen that the diffusivities leading to OH formation (at 1670 °C) and to decreased OH concentrations (at 1400–1200 °C) are four to five orders of magnitude larger compared to tracer diffusivities of lattice atoms.

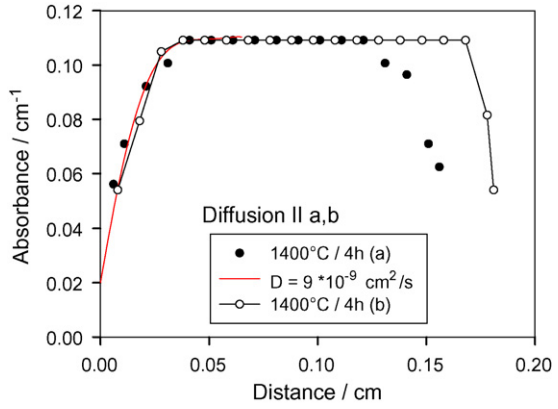

Fig. 7. Absorption profiles for diffusion components D_a (closed symbol) and D_b (open circles connected by solid line) as measured for polarization $E//a$ of cross-section cut from mullite [0 0 1] cuboids heat treated at 1400 °C/4 h, in flowing He. Thin solid line shows profile calculation using Eq. (6) and diffusion coefficient as given (note different length of specimen for D_a and D_b).

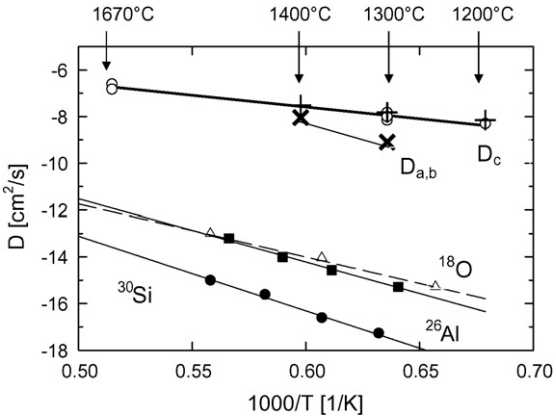

Fig. 8. Arrhenius plot of 2/1-mullite single crystal tracer diffusion coefficients of ^{30}Si (filled circle), ^{26}Al (filled square) and ^{18}O (open triangle) from Fielitz et al.,[34] OH formation at 1670 °C in H_2O rich gas and OH depletion at 1400, 1300 and 1200 °C heating under dry atmospheric conditions from Eils et al.[16] and this work (open circles and + for D_c and x for D_a, D_b). Thick solid line, thin solid lines and dashed line mark Arrhenius behaviour for, D_c-OH formation/depletion and ^{18}O, ^{26}Al, ^{30}Si tracer diffusion, respectively. Line connecting $D_{a,b}$ components at 1400 and 1300 °C indicate higher activation energy compared to E_a of D_c for OH depletion.

The data for outward diffusion can be described by an Arrhenius activated behaviour:

$$D = D_o \exp\left(-\frac{E_a}{k_B T}\right) \quad (7)$$

where k_B is the Boltzmann constant (1.38066×10^{-20} kJ/K), D_o the pre-factor ($T = \infty$ value), E_a the activation energy and T is the temperature (K), with E_a of about 197 kJ/mol (2 eV) which includes the value for inward diffusion at $T = 1670$ °C, too. Data extrapolation implies a pre-factor in the range $0.1 < D_o$ (cm^2/s) < 0.01 for the diffusion component D_c which is of the same order also obtained for ^{18}O diffusivity.[34] For diffusion perpendicular to the c axis the data imply a higher value of E_a (and D_o) which indicates a different mechanism of diffusion with a higher effective activation energy of corresponding defect formations compared to D_c. The activation energies of diffusion of ^{30}Si, ^{26}Al and ^{18}O are given by 612, 517 and 433 kJ/mol, respectively,[34] which are more than twice as large as the activation energy for diffusion of OH forming species for the D_c component.

4. Summary

Hydrogen bonding in mullite is characterized by four Lorentzian peaks for $E//a$, $E//b$ and $E//c$, respectively. The peak positions imply three different classes of hydrogen sites: (i) on tetrahedron faces with stronger hydrogen bonding; (ii) within the structural channels forming relatively isolated OH groups polarized perpendicular to the crystallographic c axis; (iii) OH dipoles strictly polarized parallel to the c axis, which are assigned to O_1–H$\cdots O_2$ pairs of corresponding oxygens in two neighboring cells along c. Lattice calculations show energetically favorable proton localization for the first two cases. Polarized infrared spectra for the structurally closely

related natural mineral sillimanite support earlier results.[30,31] The peaks of much stronger absorption intensities for sillimanite compared to mullite which are also at different peak positions are explained with coupled substitutions involving transition metal impurities. The weaker absorptions characteristics in the sillimanite spectra in the range between 3400 and 3600 cm^{-1} are similar to those obtained for mullite.

Hydrogen diffusion shows a significant anisotropy $D_c > D_a \approx D_b$ evaluated for depletion of OH bonds in dry atmospheric conditions at 1400 and 1300 °C. Arrhenius activation energy for hydrogen diffusion parallel to the *c* axis is about 192 kJ/mol when the data obtained for inward diffusion at 1670 °C are included, suggesting the same mechanism in both cases. For diffusion parallel to *a* and *b* a higher activation energy is indicated implying a different mechanism. The tracer diffusivities of the lattice species ^{18}O, ^{26}Al and ^{30}Si were related to appropriate vacancy formations $[V'''_{Si}]$, $[V'''_{Al}]$, and $[V_O^{\bullet\bullet}]$ (Kröger–Vink notation)[34] which requires more than twice as much in activation energy compared to the activation energy necessary for hydrogen diffusion along *c*. Therefore hydrogen diffusion mechanism for D_c may involve a coupled mechanism of vacancy formation enabling an enhanced effective proton diffusion which is related to the structural channels along *c*.

Acknowledgements

We thank the "Deutsche Forschungsgemeinschaft" (DFG, Schn 297/25-1) for financial support, S. Uecker (Institute for Crystal Growth, Berlin-Adlershof, Germany) for the preparation of the mullite single crystals and O. Diedrich (Institute of Mineralogy, Leibniz University of Hannover) for preparing the oriented single crystal cuts.

References

1. Wilkins, R. W. T. and Sabine, W., Water content of some nominally anhydrous silicates. *Am. Mineral.*, 1973, **58**, 508–516.
2. Beran, A., Messung des Ultra-Pleochroismus von Mineralen. XIV. Der Pleochroismus der OH-Streckfrequenz im Diopsid. *Tschermarks Min. Petr. Mitt.*, 1976, **35**, 19–25.
3. Skogby, H. and Rossman, G. R., OH^- in pyroxene: an experimental study of incorporation mechanism and stability. *Am. Mineral.*, 1989, **75**, 764–774.
4. Bell, D. R. and Rossman, G. R., Water in the Earth mantle: the role of nominally anhydrous minerals. *Science*, 1992, **255**, 1391–1397.
5. Langer, K., Robarick, E., Sobolev, N. V., Shatsky, V. S. and Wang, W., Single crystal spectra of garnets from diamondiferous high-pressure metamorphic rocks from Kazakhstan: indications for OH^-, H_2O, and FeTi charge transfer. *Eur. J. Mineral.*, 1993, **5**, 1091–1100.
6. Mackwell, S. J., Kohlstedt, D. L. and Paterson, M. S., The role of water in deformation of olivine single crystals. *J. Geophys. Res.*, 1985, **90**, 11319–11333.
7. Hirth, G. and Kohlstedt, D. L., Water in the oceanic upper mantle: implications for rheology, melt extraction, and the evolution of the lithosphere. *Earth Planet. Sci. Lett.*, 1996, **14**, 93–108.
8. Ingrin, J. and Skogby, H., Hydrogen in nominal anhydrous upper-mantle minerals: concentration levels and implication. *Eur. J. Mineral.*, 2000, **12**, 543–2000.
9. Keppler, H. and Smyth, J. R., ed., Water in nominally anhydrous minerals. *Rev. Mineral. Geochem.*, 2006, **62**, 1–473.
10. Kronenberg, A. K., Hydrogen specifications and chemical weakening of quartz. *Rev. Mineral. Ser.*, 1994, **29**, 123–176.
11. Kronenberg, A. K., Castaing, J., Mitchell, T. E. and Kirby, S. H., Hydrogen defects in α-Al_2O_3 and water weakening of sapphire and alumina ceramics between 600 and 1000 °C. I. Infrared characterization of defects. *Acta Mater.*, 2000, **48**, 1481–1494.
12. Castaing, J., Kronenberg, A. K., Kirb, S. H. and Mitchell, T. E., Hydrogen defects in α-Al_2O_3 and water weakening of sapphire and alumina ceramics between 600 and 1000 °C. I. Mechanical properties. *Acta Mater.*, 2000, **48**, 1495–1504.
13. Schneider, H., Okada, K. and Pask, J. A., *Mullite and Mullite Ceramics*. John Wiley and Sons, 1994.
14. Schneider, H. and Komarneni, S., ed., *Mullite*. Wiley VCH, Weinheim, 2005.
15. Rüscher, C. H., Shimada, S. and Schneider, H., High-temperature hydroxylation of mullite. *J. Am. Ceram. Soc.*, 2002, **85**, 1616–1618.
16. Eils, N., Rüscher, C. H., Shimada, S., Schmücker, M. and Schneider, H., High temperature hydroxylation and surface corrosion of 2/1-mullite single crystals in water vapor environments. *J. Am. Ceram. Soc.*, 2006, **89**, 2887–2894.
17. Rüscher, C. H., Eils, N., Horn, I., Schneider, H. and Shimada, S., Corrosion of mullite in contaminated water rich gas mixtures at high temperatures: the effect of impurity diffusion. *Advances in Science and Technology*, *Vol. 45*. Trans Tech Publications, Switzerland, 2006, pp. 167–172.
18. Schmalzried, H., *Chemical Kinetics of Solids*. VCH Verlagsgesellschaft, Weinheim, 1995, pp. 364–365.
19. Nakamoto, K., Margoshes, M. and Rundle, R. E., Stretching frequencies as a function of distances in hydrogen bonds. *J. Am. Chem. Soc.*, 1955, **77**, 6480–6488.
20. Novak, A., Hydrogen bonding in solids. In *Structure and Bonding*, *Vol. 18*, ed. J. D. Dunitz, P. Hemmerich, R. H. Holm, J. A. Ibers, C. K. Jorgensen, J. B. Neilands, D. Reinen and R. J. P. Williams. Springer, New York, 1974, pp. 177–216.
21. Kubicki, J. D., Sykes, D. and Rossman, G. R., Calculated trends of OH infrared stretching vibrations with composition and structure in aluminosilicate molecules. *Phys. Chem. Miner.*, 1993, **20**, 425–432.
22. Libowitzky, E., Correlation of O–H stretching frequencies and O–H···O hydrogen bond lengths in minerals. *Monatshefte für Chemie*, 1999, **130**, 1047–1059.
23. Rüscher, C. H., Phonon spectra of 2:1 mullite in infrared and Raman experiments. *Phys. Chem. Miner.*, 1996, **23**, 50–55.
24. Rüscher, C. H., Thermic transformation of sillimanite single crystal to 3:2 mullite plus melt: investigations by polarized IR-reflection micro spectroscopy. *J. Eur. Ceram. Soc.*, 2001, **21**, 2463–2469.
25. Rüscher, C. H., Mileiko, S. T. and Schneider, H., Mullite single crystal fibres produced by the internal crystallization method (IMC). *J. Eur. Ceram. Soc.*, 2003, **23**, 3113–3117.
26. Libowitzky, E. and Rossman, G. R., An IR absorption calibration for water in minerals. *Am. Mineral.*, 1997, **82**, 1111–1115.
27. Libowitzky, E. and Rossman, G. R., Principles of quantitative absorbance measurements in anisotropic crystals. *Phys. Chem. Miner.*, 1996, **23**, 319–327.
28. Angel, R. J. and Prewitt, C. T., Crystal structure of mullite: a re-examination of the average structure. *Am. Mineral.*, 1986, **71**, 1476–1482.
29. Stalder, R., Influence of Fe, Cr and Al on hydrogen incorporation in orthopyroxene. *Eur. J. Mineral.*, 2004, **16**, 703–711.
30. Beran, A., Hafner, St. and Zeman, J., Untersuchungen über den Einbau von Hydroxilgruppen im Edelstein-Sillimanit. *Neues Jahrbuch für Mineralogie Monatshefte*, 1983, 219–226.
31. Beran, A., Rossman, G. R. and Grew, E. S., The hydrous component of sillimanite. *Am. Mineral.*, 1989, **74**, 812–817.
32. Gale, J. D., GULP—a computer program for the symmetry adapted simulation of solids. *JCS Faraday Trans.*, 1997, **93**, 629.
33. Fritze, H., Jojic, J., Wilke, T., Rüscher, C. H., Weber, S., Scherrer, S., Weiss, R., Schultrich, B. and Borchardt, G., Mullite-based oxidation protection for SiC–C–C composites in air at temperatures up to 1900 K. *J. Eur. Ceram. Soc.*, 1998, **18**, 2351–2364.
34. Fielitz, P., Borchardt, G., Schmücker, M. and Schneider, H., A diffusion-controlled mullite formation reaction model being based on tracer diffusivity data of aluminium, silicon and oxygen. *Philos. Mag.*, 2007, **87**, 111–127.